Peer-reviewed version available at Biosensors 2017, 7, 55; doi:10.3390/bios7040055

Article

A Radar-based Smart Sensor for Unobtrusive Elderly Monitoring in Ambient Assisted Living Applications

Giovanni Diraco [1,*], Alessandro Leone [2] and Pietro Siciliano [3]

[1] National Research Council of Italy, Institute for Microelectronics and Microsystems, Lecce; giovanni.diraco@le.imm.cnr.it
[2] National Research Council of Italy, Institute for Microelectronics and Microsystems, Lecce; alessandro.leone@le.imm.cnr.it
[3] National Research Council of Italy, Institute for Microelectronics and Microsystems, Lecce; pietro.siciliano@le.imm.cnr.it
* Correspondence: giovanni.diraco@le.imm.cnr.it; Tel.: +39-832-422-533

Abstract: Continuous in-home monitoring of older adults living alone aims to improve their quality of life and independence, by detecting early signs of illness and functional decline or emergency conditions. To meet requirements for technology acceptance by seniors (unobtrusiveness, non-intrusiveness, privacy-preservation), this study presents and discusses a new smart sensor system for the detection of abnormalities during daily activities, based on ultra-wideband radar providing rich, not privacy-sensitive, information useful for sensing both cardiorespiratory and body movements, regardless of ambient lighting conditions and physical obstructions (through-wall sensing). The radar sensing is a very promising technology, enabling the measurement of vital signs and body movements at a distance, and thus meeting both requirements of unobtrusiveness and accuracy. In particular, impulse-radio ultra-wideband radar has attracted considerable attention in recent years thanks to many properties that make it useful for assisted living purposes. The proposed sensing system, evaluated in meaningful assisted living scenarios by involving 30 participants, exhibited the ability to detect vital signs, to discriminate among dangerous situations and activities of daily living, and to accommodate individual physical characteristics and habits. The reported results show that vital signs can be detected also while carrying out daily activities or after a fall event (post-fall phase), with accuracy varying according to the level of movements, reaching up to 95% and 91% in detecting respiration and heart rates, respectively. Similarly, good results were achieved in fall detection by using the micro-motion signature and unsupervised learning, with sensitivity and specificity greater than 97% and 90%, respectively.

Keywords: fall detection; vital signs monitoring; ultra-wideband radar; micro-Doppler

---

1. Introduction

Besides being the fastest growing sector [1], the population aged 65 and over suffers the greatest number of falls causing emergency visits for trauma, hospitalizations and injury deaths [2, 3], as well as age-related health disorders (e.g., illness or functional decline [4]). Thus, in the context of assisted living, there is an increasing demand for unobtrusive sensing of human activities and behaviors as well as physiological parameters, suitable for detection of dangerous situations and even for early prediction of health disorders, in order to actually provide timely medical assistance and alerts to caregivers. As some studies pointed out [5, 6, 7], the so called long-lie after a fall (more than one hour) increases risk of both hospitalization and death. Automatic fall-detection systems, saving time for the arrival of medical assistance, have the potential to reduce risk of these adverse health consequences [8]. On the other hand, respiration rate (RR) and heart rate (HR) are fundamental physiological parameters whose alterations may be correlated, especially during ageing, with the progress of physical illnesses (e.g., sleep-disordered breathing [9], congestive heart failure [10], subclinical inflammation [11]) as well as mental and neuro-degenerative diseases (e.g., major depressive disorder [12], Parkinson disease [13, 14]).

Nevertheless, in this context, the emphasis on unobtrusiveness is especially important. In fact, as it has been assessed in [15], older adults are more likely to accept in-home sensing technologies when these are unobtrusive, i.e., they do not demand to wear any device, not interfere with daily life, not require to learn new technical skills and, above all, not capture video images. By the way, it is only by means of a good acceptability that it is possible to provide a continuous monitoring, essential to produce long-term health data from which informative patterns can be extracted. Furthermore, fall-detection and health monitoring solutions are evaluated not only on the basis of their detection performance, usually expressed in terms of accuracy, sensitivity and specificity, but also (or even more so) on the basis of their acceptability by end-users. Essentially, the main issues of such systems can be traced to the adopted sensing technology and detection methodology.

1.2. Sensing technology

Existing solutions can be roughly categorized on the basis of the positioning modality of their sensing elements. The golden standard for measurement of the heart activity is the electrocardiograph (ECG) [16], which involves various kind of electrodes (i.e., conventional Ag–AgCl suction, adhesive gel, etc.) attached to the skin on the chest and limbs. Whereas in regards to the respiration activity, the standard measurement technique is the transthoracic impedance plethysmography (IP), requiring skin electrodes placed on the chest of which at least two must be ECG electrodes [17].

Focusing on the measurement of basic parameters, such as respiration-rate (RR) and heart-rate (HR), slightly more comfortable approaches may involve the use of textile dry or capacitive ECG electrodes, elastic bands around abdomen and/or chest (e.g., respiratory inductance plethysmography), optoelectronic sensors (e.g., Photoplethysmography - PPG), and even pressure or accelerometer sensors. However, all these approaches still require the subject to be tethered to a body-worn or closely located measurement device, resulting uncomfortable and unpractical for continuous monitoring in assisted living scenarios. Remote sensing techniques offer a more suitable alternative by which RR and HR can be unobtrusively detected and measured at a distance (ranging from tens of centimeters to meters). Such techniques may exploit either optical or radio waves, leading to camera-based photoplethysmography (cbPPG) and radar sensing, respectively. The working principle of cbPPG is to detect small changes in the skin color due to cyclic variations of blood volume in arteries and capillaries under skin, and thus to estimate the PPG signal which is proportional to such skin color changes [18]. Instead, the remote sensing of vital signs using radar is based on detection of small movements induced by the heartbeat and respiratory chest-wall motions [19]. The cbPPG technique, unlike the radar-based one, allows to estimate also the blood oxygen level (SpO2), but radar sensing is more accurate in estimation of RR and HR (particularly in presence of multiple heartbeats and cluttered scenarios with obstacles) [20].

Regarding the fall-detection solutions, they can be categorized into wearable solutions which require the user wears some device, and ambient solutions which can be further categorized in contact and contactless. The wearable device can be a simple manually-operated Personal Emergency Response System (PERS), not useful however in case of loss of consciousness, or an automatic system equipped with on-body motion sensors such as accelerometers, gyroscopes, and compasses. Wearable solutions can be used “on the move” and show relatively good detection performance, but their common drawbacks are the limited battery life, the need for on-board processing and/or wireless communication (both energy-demanding functions), the inconvenience of having to remember to wear a device and the discomfort caused by the device itself.

On the other hand, contact ambient solutions require the installation of sensing elements in proximity of surfaces involved in the fall impact. They can be simple switches, or pressure and vibration sensors embedded in carpets and flooring. Such solutions, disappearing in the environment, are generally well-accepted by end-users. Conversely, their detection performance

Preprints (www.preprints.org) | NOT PEER-REVIEWED | Posted: 17 October 2017 doi:10.20944/preprints201710.0115.v1

Peer-reviewed version available at Biosensors 2017, 7, 55; doi:10.3390/bios7040055

depends on the number and careful positioning of sensors, which may require modification or redesign of the home environment.

Regarding contactless solutions, they usually adopt sensors able to work remotely, mounted on wall or ceiling of a room. In the case of acoustic and visual sensing, microphones and cameras are respectively used to perform some kind of scene analysis. Those based on camera are the most highly performing and extensively investigated solutions, although they may raise significant privacy concerns. Range sensing is a contactless modality based on the remote measurement of distances. Commonly employed sensors are pyroelectric infrared (PIR), Sonar, Lidar, Range camera, and Radar. Acceptability and performance are quite good, especially in the case of Range camera and Radar.

Although Ultra-Wideband (UWB) Radar sensing can exploit either Continuous Wave (CW) or Impulse Radio (IR) architectures, the second one is particularly interesting [21] since it leads to a single device whose capabilities include: measurement of vital parameters, target detection and localization, through-wall imaging (high penetration power) and secure high-throughput wireless communication [22]. Although poorly investigated for fall detection (i.e., UWB-CW Radar is almost universally adopted [23]), such capabilities make the UWB-IR Radar a promising multi-purpose technology for unobtrusive in-home monitoring and assisted living applications. Furthermore, it is a fully privacy-preserving sensing technology, since captured information is outside the human sensory capabilities (unlike cbPPG and cameras in general that capture images), and thus not directly usable for obtaining privacy-sensitive information.

1.3. Detection methodology

The widely adopted fall-detection methodologies use supervised algorithms, in which a dataset including both falls and non-fall actions (e.g., walking, sitting, etc.) need to be collected in order to set up the detection algorithm. Normally, collected actions are performed by healthy, and often young, volunteers. A part of collected data is used for training, the rest for testing and validation. The weakness of supervised approaches lies in the need of a fall-based training. It is not so straightforward that, when the system will be used in the field by older adults, the performance will be the same as that achieved using simulated falls.

As an alternative methodology, unsupervised algorithms can be set up in the field and customized to end-user's characteristics. This is done by following a complementary approach with respect to the past, consisting in training (or calibrating) algorithms in order to recognize "usual" actions, such as walking, sitting, resting on the bed, and so on. After the training, falls are detected as anomalies with respect to observed actions. In spite of their versatility, very few studies have investigated unsupervised approaches. To the best of the author's knowledge, the studies that attempted to do so have used data provided by wearable [24, 25, 26, 27] or acoustic [28] sensors, whereas there are no studies in the literature that used Radar sensing to detect falls via unsupervised approach.

2. Materials and Methods

The purpose of this study was to develop and validate a Radar Smart Sensor (RSS) able to detect both cardiorespiratory and body movements without causing any discomfort to older adults. In the remainder of this section, the system architecture is gradually detailed, starting with a general overview and then describing each system parts, with major focus on micro-Doppler processing, micro-movement signature definition, and vital signs estimation via Empirical Mode Decomposition (EMD). Finally, the experimental setup and validation procedure are presented.

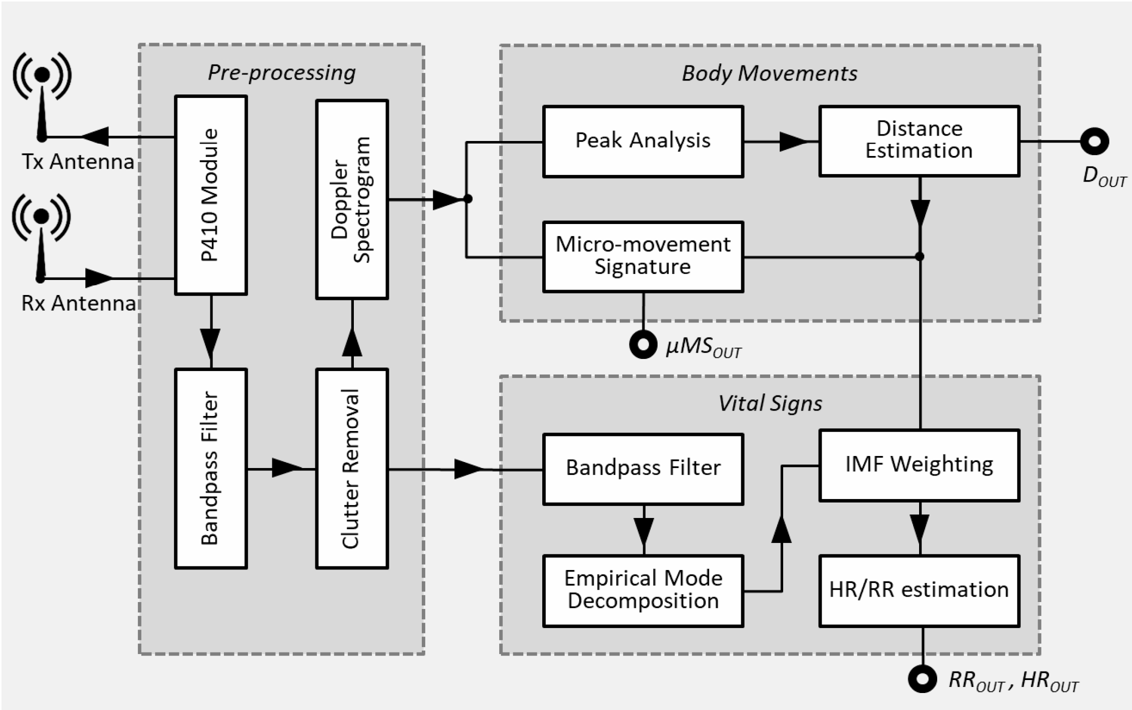

Figure 1. RSS system overview.

2.1. System Overview

The detection system, of which a schematic representation is given in Figure 1, is composed of the three main stages: 1) Pre-processing; 2) Body movements; 3) Vital signs. The pre-processing receives signals from the radar unit (i.e., the P410 module) and provides signal processing functions useful for the other two stages of the systems. The “body movements” stage is devoted to the computing of micro-motion signatures (μMS) and distances between body and antenna (D), starting from the Doppler-spectrogram provided by the “pre-processing stage.” The third stage, “vital signs,” received the clutter-free signal as input estimates the HR and RR, using also the distance information computed by the “body movements stage.” The aforementioned main stages are further detailed in the following sections.

2.2. Pre-processing

2.2.1. Radar module

Radar systems can be categorized on the basis of their radio-wave bandwidth into: narrowband (NB) and UWB. The UWB is a radio technology using either pulse (IR) or CW of very short duration, and operating on frequency range wider than 500MHz or 25% of the center frequency. More specifically the UWB-IR, operating over a larger bandwidth and wider range of frequencies [21], provides additional features over UWB-CW, particularly useful in AAL (Ambient Assisted Living) contexts. The sub-millimeter range resolution and high penetration power enable the detection of very small target event through obstacles (e.g., through-wall sensing of vital signs). The shorter pulse duration, lower than the total travel time of the wave even in case of multiple reflections, is helpful to deal with multipath effects particularly insidious in indoor environments. The very low power spectral density prevents interferences with other radio systems operating in the same frequency range, and guarantees a low probability of interception; enabling secure high-data-rate communication in short range (e.g., up to 500Mbps@3m).

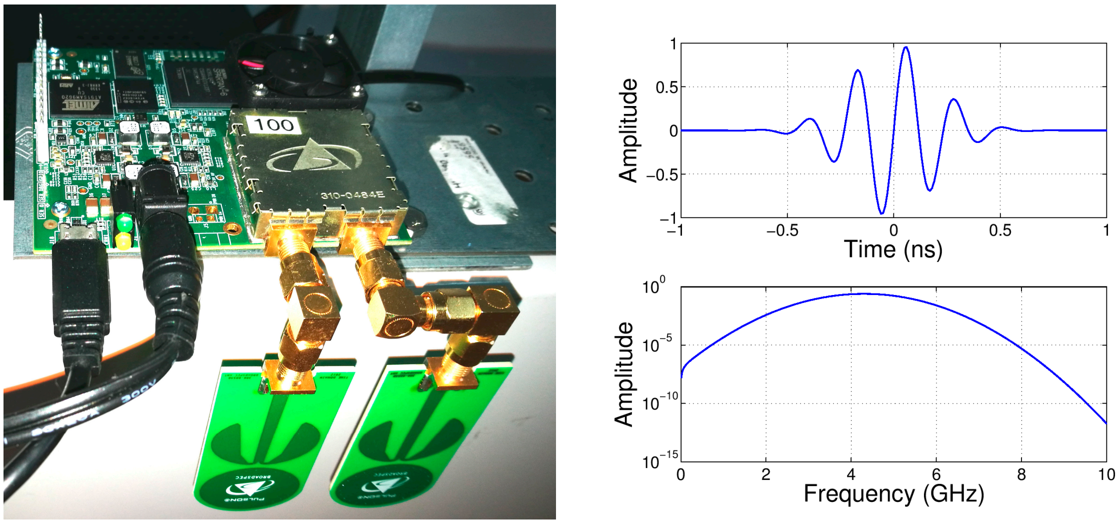

(a) (b)

Figure 2. a) P410 radar module, and b) P410 Pulse waveform (top-side) and related frequency spectrum (bottom-side).

The Time Domain PulsON P410 [29], reported in Figure 2.a, is a state-of-the-art UWB-IR radar module, enabling precise measurements in high multipath and high clutter environments. The P410 is characterized by low cost, small size (7.6×8.0×1.6 cm board dimensions), as well as low power operation (from -33 to -13 dBm) conforming to FCC requirements; all made possible by a dedicated UWB chipset, which includes various software-configurable parameters useful for application customization. The pulse waveform is a bandpass signal with frequency spectrum 3.1-5.3 GHz centered at 4.3 GHz, as exemplified in Figure 2.b, generated at a pulse repetition rate of 10 MHz, and received at sampling rate of 61 ps.

The Monostatic Radar Module (MRM) receiver architecture of the radar module adopted in this study is represented in Figure 3. The radar scan data are converted into bins, each of 1.907 ps, at increments of 32 bins (i.e., fast-time sampling time of 61 ps) and stacked into 96 readings covering 5859.36 ps. Hence, starting and ending scan times, T1 and T2, which are directly related with distance range R1 and R2, must be selected such as their difference is a multiple of 5859.36 ps. The receiver architecture, based on several parallel samplers (i.e., rake receiver architecture), allows the integration of multiple scans S_k in order to improve the SNR (Signal-to-Noise Ratio) of radar returns. The minimum number of integrated scans is 64 (i.e., 2^6) corresponding to a SNR increase of 18 dB which further increases of 3 dB at each doubling of integrated scans, up to a maximum of 32768 (i.e., 2^{15}) scans, i.e., 45 dB. The time duration t_s of a full scan depends on the number of integrations, computed as 2^{PII} where PII is the Pulse Integration Index ranging from 6 to 15, and on the distance range (i.e., the size of the scan window T2-T1), as follows: $t_s = 0.792 \cdot 2^{PII} \cdot \mathrm{Round}\left(\frac{T2-T1}{5859.36}\right)$ (μs).

Table 1. P410 MRM rake receiver architecture.

T1	T2	R1	R2	N	PII	dB	Fr (Hz)	ts (μs)	ti (μs)
13334	19193	0.5	1.38	96	12	36	50	3244.03	16755.97
13334	25053	0.5	2.26	192	12	36	50	6488.06	13511.94
13334	30912	0.5	3.13	288	12	36	50	9732.10	10267.90
13334	36771	0.5	4.01	384	12	36	50	12976.13	7023.87
13334	42631	0.5	4.89	480	12	36	50	16220.16	3779.84
13334	48490	0.5	5.77	576	12	36	50	19464.19	535.81

Preprints (www.preprints.org) | NOT PEER-REVIEWED | Posted: 17 October 2017 doi:10.20944/preprints201710.0115.v1

Peer-reviewed version available at Biosensors 2017, 7, 55; doi:10.3390/bios7040055

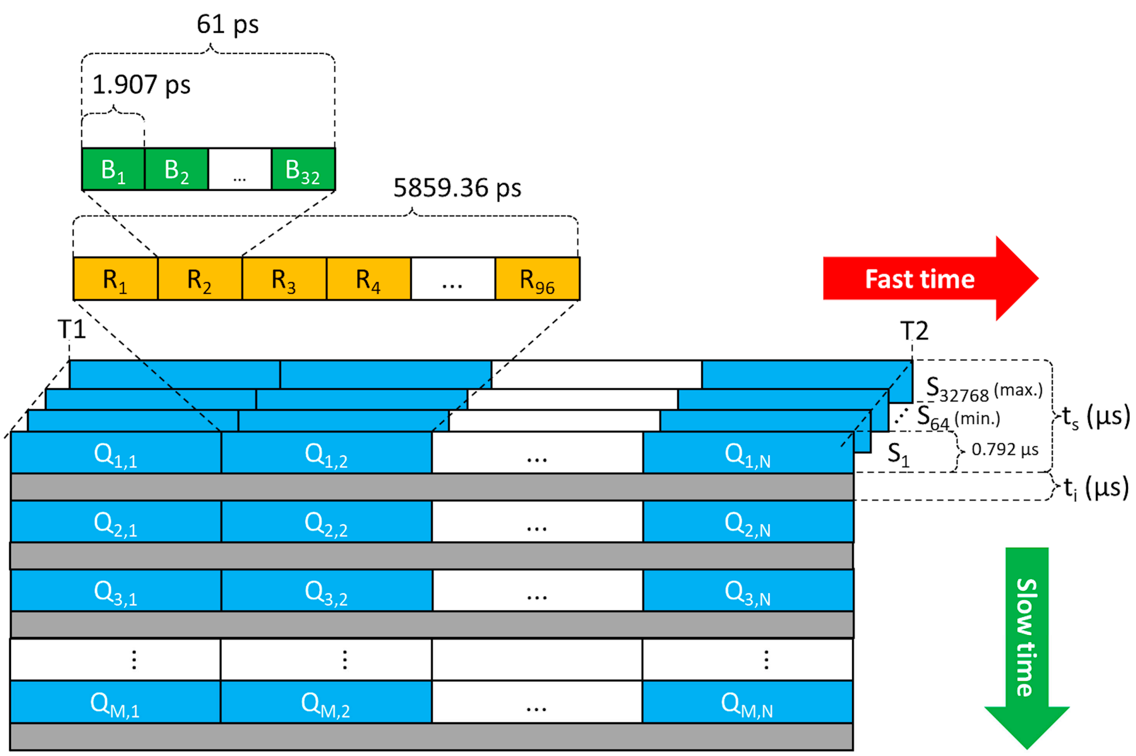

Figure 3. P410 MRM rake receiver architecture.

In addition, between one scan and another, there is a further time interval t_i, so that the slow-time sampling frequency is given by $F_s = t_s + t_i$. In the present study, the previously design parameters were selected in order to cover a distance range from R1=0.5 m to R2=5.77 m, at sampling frequency of 50 Hz and with 36 dB of increase in the SNR. All selected parameters are summarized in Table 1.

2.2.2. Bandpass filtering

Interference and noise due to various types of sources may cause undesirable signal degradation. In presence of wideband sources, the related noise has the form of short random pulses which can be significantly attenuated by integrating (and averaging) multiple received signals, thanks to the, previously described, rake receiver architecture. Instead, in the case of narrowband sources, which mainly are nearby systems generating electromagnetic interference with sinusoidal waveform and random amplitudes, usually a bandpass filtering is used to attenuate this type of noise. To this end, in the present study, the received radar signal was filtered by a 16th-order Butterworth with bandpass in the radar operating frequency range, i.e., from 3.1 to 5.3 GHz.

2.2.3. Clutter removal

Beside noise and interference, the clutter is another problem which may reduce the SNR of radar returns. The clutter returns are unwanted signal components induced by reflection from static structures included in the environment (i.e., walls, furniture), and whose energy can be several orders magnitude larger than the useful signals reflected from the person's body (e.g., torso, limbs, chest cavity, etc.).

The clutter removal stage is devoted to the attenuation of those signals, by using a Singular Value Decomposition (SVD) [30] based approach. Following this approach, the signal matrix was SVD decomposed obtaining a diagonal matrix whose first 'few' descending-ordered singular values

Peer-reviewed version available at Biosensors 2017, 7, 55; doi:10.3390/bios7040055

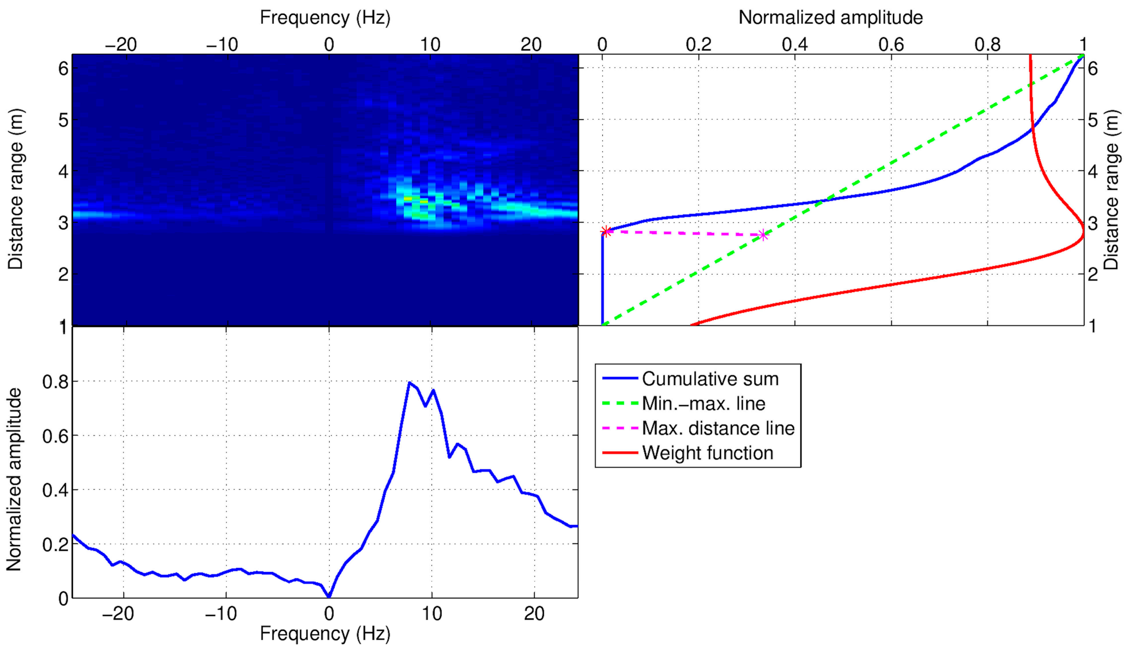

Figure 4. Doppler spectrogram (top-left image) from which the body position (i.e., distance from the radar antenna) is estimated (top-right image), and the micro-motion signature extracted (bottom-left image).

conveyed the largest amount of clutter energy. By setting these singular values to zero and reconstructing the signal matrix, the clutter energy was removed and the SNR improved.

2.2.4. Micro-Doppler spectrogram processing

The Doppler spectrogram was used first for estimating the distance of the person's body from the radar, and then for extracting the micro-motion signature useful for both person localization and activity recognition. The body position was estimated by projecting the spectrogram on the distance range. After that, the micro-motion signature was obtained by projecting the Doppler spectrum on frequencies, but restricted to the only region of the distance range including the estimated body position. Both procedures are exemplified in Figure 4. The Doppler spectrogram was computed by applying the discrete-time Fourier transform (DTFT) to the analytic version of the clutter-free signal, i.e., the output signal provided by the clutter removal module. (As well known the analytic signal is a complex signal obtained by setting the imaginary part to be equal to the Hilbert transform of the original real signal [31].) The DTFT length was fixed to N=16, for computational efficiency reasons, to which corresponded a time duration of $T_{DTFT} = \frac{N}{Fr} =$ 320ms by considering a short-time sampling frequency of Fr=50Hz. As an example, the Doppler spectrum related to a walking action is depicted in Figure 4 (top-left image).

2.3. Body movements

As mentioned above, the estimation of body movements consisted of two main steps. The first step was to estimate the distance between the (closest) person and the radar sensor. The second step was to extract a micro-motion signature by considering the only spectrogram region located at the previously estimated distance.

In order to estimate the person-radar distance d, the spectrogram was projected on the distance axis by taking the cumulative sum over distances (solid blue line in the top-right part of Figure 4). Hence, the maximum curvature change was estimated as the farthest point from the line joining the minimum and maximum points (green dotted line in the top-right part of Figure 4), and the corresponding point on distance range was considered as distance d (just under 3 m in the example of Figure 4).

Since, in general, the spectral content is not uniformly spread over the spectrogram, but on the contrary it is confined in the range region interested by the body's movement (e.g., the range above 3 m in Figure 4), to improve the SNR a special sigmoidal-shaped function was considered (solid red line in the top-right part of Figure 4) having the following analytical expression: $h(x) = 4\frac{1+\tanh x}{(2+\tanh x)^2}$. The property of this function is that it does not decay uniformly after the curvature change but instead it maintains a high gain level for a while, after that it rapidly declines to a constant value. Then, the spectral region related to body's movements was filtered by multiplying the spectrogram by the response function $H(f,x) = h(x-d)$ with f varying in frequency domain and x in distance range. Finally, the micro-motion signature μ-MS was extracted from the filtered spectrogram as average summation over frequencies (solid blue line in the bottom-left part of Figure 4). The average was calculated by taking N_S (50%-overlapped) DTFTs, thus covering a time window of $T_S = \frac{N_S+1}{2}T_{DTFT}$ per signature. The optimal N_S was determined using ROC (Receiver-Operating Characteristic) analysis.

It is important to note that the combined peak analysis of both micro-motion signature μ-MS and distance d (over fast-time and slow-time, respectively) allowed to discriminate the regions of the spectrogram in which body movements were more intense from those where they were less

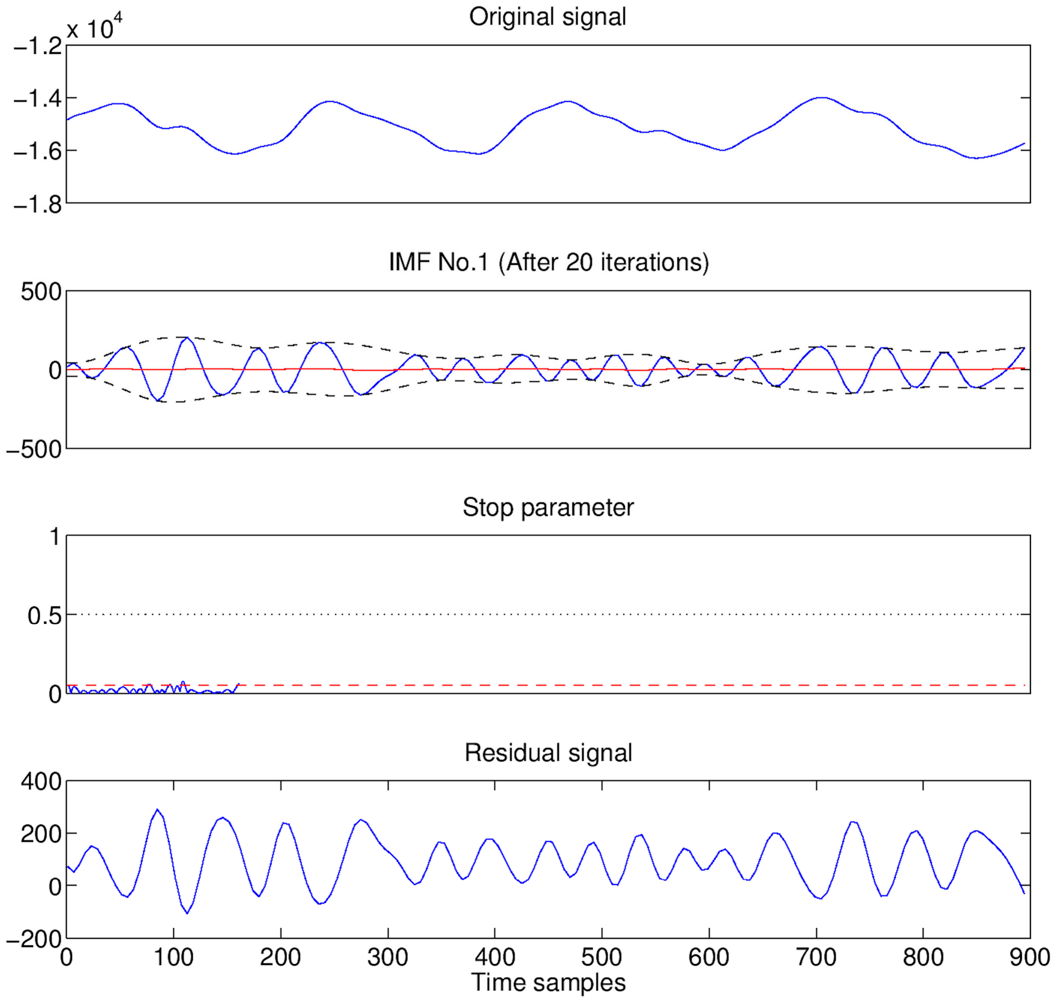

Figure 5. Extraction process of the first IMF (the 20th iteration) from a radar signal via EMD procedure.

intense, and thus provided an effective strategy for movement compensation during the estimation of vital signs.

2.4. Vital signs

Since the SNR of radar returns reflected from the monitored subject's chest, and useful for vital signs estimation, can be affected by unwanted signals or noise (e.g., generated by periodic sources such as fans, motors, curtains/doors motion, etc.), thus a second bandpass filter was implemented, namely, a 6th order IIR Butterworth in slow-time with a passband from 0.125 Hz (corresponding to a minimum of 7.5 breaths/min) to 3 Hz (corresponding to a maximum HR of 180 beats/min).

The filtered signal was, hence, decomposed into simpler signals, named intrinsic mode functions (IMFs), using Empirical Mode Decomposition (EMD) [32]. The EMD is an iterative approach which aims to extract the various simple mode oscillations of a signal $s(t)$ at a very local level, performing the extraction process summarized in the following steps, and also illustrated in Figure 5.

1) Find all maxima (minima) of $s(t)$ and interpolate them with cubic splines. This produces the upper envelope $e_U(t)$ (lower envelope $e_L(t)$). (See the second plot in Figure 5)
2) Compute the residual signal as mean of the two envelops, i.e., $m(t) = \frac{e_U(t)+e_L(t)}{2}$.
3) Extract the local detail as $d(t) = s(t) - m(t)$.

The previous steps are iterated upon the detail $d(t)$ until the latter has not exactly one zero between any two consecutive local extrema (known as sifting process). When this stop criterion is satisfied, $d(t)$ can be considered as an IMF and the three steps are iterated on the residual signal $m(t)$. The extraction process stops when $m(t)$ is close to zero (i.e., the mean is below a given threshold).

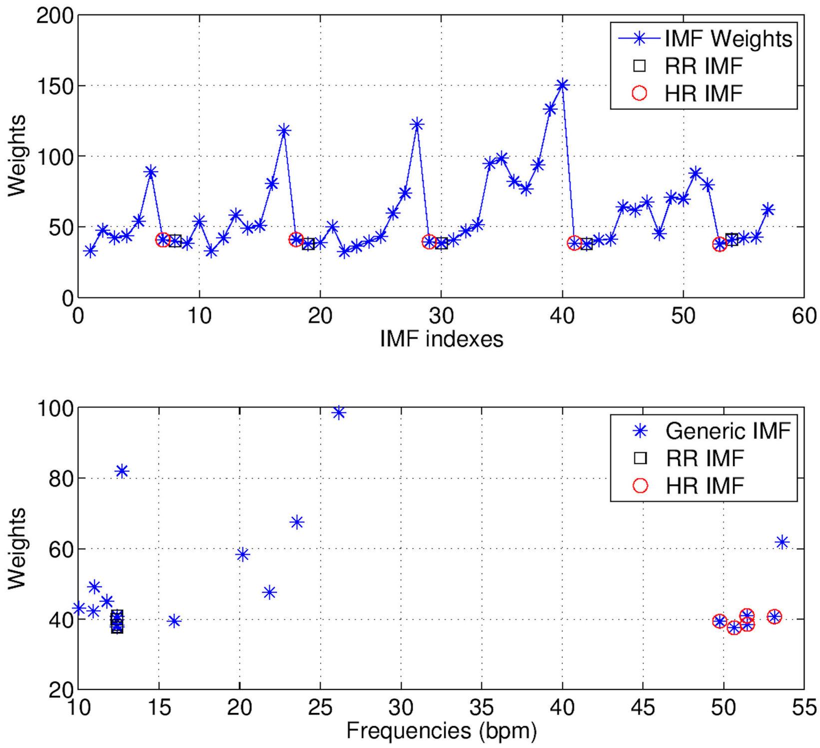

Figure 6. Selection strategy of the IMFs which best describe the cardiorespiratory signal. The selected IMFs are related with the minimum weights immediately following the local maxima (the upper plot in this figure). Finally, the HR and RR are estimated as average frequencies of the selected IMFs (the lower plot in this figure).

Figure 7. Final assembly of the RSS, suitable for tripod mounting.

As discussed in the previous subsection, body movements interest only a limited portion of the distance range. Let $D = \{d \mid D1 \leq d \leq D2\}$ be the current, or the latest region, in which movements (closest to the sensor) have been detected. For example, referring to Figure 4, the interested range is delimited by $D1$=3m and $D2$=4m. Given an observation time window of size T, a certain number of radar scans s_k, confined in D, can be decomposed via EMD in n_k modes, namely $M_k = \{f_{k,j} \mid \forall j = 1, \dots, n_k\}$, as previously detailed.

In order to be able to estimate HR and RR from extracted modes, a weight $w_{k,j}$ was assigned to each $f_{k,j}$ so that $w_{k,j} = \left\| \mathrm{pdf}(s_k) - \mathrm{pdf}(f_{k,j}) \right\|_2$, where $\mathrm{pdf}(\cdot)$ is the probability density function (PDF) approximated with an histogram of bin size equal to $\max\{\mathrm{std}(s_k) \mid \forall k \in K\}/4$, $\mathrm{std}(\cdot)$ is the standard deviation, and $\|\cdot\|_2$ is the L2-norm which has been reported to be one of the most efficient similarity measure for identifying the relevant modes of a signal [33]. The weight sequence $\{w_{1,1}, w_{1,2}, \dots, w_{1,n_1}, w_{2,1}, w_{2,2}, \dots, w_{2,n_2}, \dots\}$ was used to identify the IMFs that best described the signal (i.e., the cardiorespiratory signal).

The IMF selection strategy can be intuitively explained by observing the "up and down" behaviour of the weight sequence, as illustrated in the example shown in Figure 6. For each scan s_k the related weight subsequence $\{w_{k,1}, w_{k,2}, \dots, w_{k,n_k}\}$ increases until the last noisy mode (local maximum), then it decreases until its minimum value corresponding to the IMFs that best describe the signal.

2.5. Experimental setup and validation

All previously discussed processing modules were developed in C language and ran on an Embedded PC (EPC), with 1.6 GHz Intel® Atom™ Processor Z530 and 2 GB RAM, namely the eBOX530-820-FL manufactured by Axiomtek [34], having compact dimensions of about 132 × 95.4 × 47.5 mm and low power consumption of 25 W. Both EPC and radar module were assembled together into a unique compact structure including also a back reflector to the radar antennas which reduced the azimuth pattern to around 100° (i.e., detection restricted to a zone at the anterior of the antenna). A picture of the resulting RSS is shown in Figure 7.

The validation experiments were conducted in the laboratory setting by involving 30 healthy subjects divided into two age groups of avg. 25 and 47 years old, respectively. Each participant simulated various types of ADLs, such as cooking, preparing meals, washing dishes, eating at the kitchen table, sitting on the couch watching TV, resting in bed, doing physical activities. The aforesaid ADLs were grouped in 15 sequences of 900 sec. (15 min.) in duration per participant. Additionally, after each sequence, the participants performed various falls in four different directions, i.e., forward, backward, lateral left/right, as suggested by Nuory et al. [35]. To this end, the two participant groups were separately instructed by geriatricians on how falls should be

Peer-reviewed version available at Biosensors 2017, 7, 55; doi:10.3390/bios7040055

realistically simulated. Hints from studies on real-life fall events were also taken into account [36, 37]. This simulation protocol, which included also the use of protective devices such as padded mat and knee protection, was preventively approved by the local ethics committee.

As reported in Figure 8, the data collection were performed in a laboratory room of about 5.8 m × 3.8 m equipped with the following furniture parts: table, chair, bed and inflatable mat. All furniture parts were easily movable, allowing to simulate ADLs and falls at different distance from the RSS within a distance range of about 5 m and different orientations. The RSS was mounted on a tripod at the far end of the room, at two different heights above the floor, namely 1.20 m and 2.40 m.

The detection performance was evaluated also in presence of multiple, moving people. At this purpose the acquisition sequence was approximatively divided into two parts: during the first part the participants stayed alone in the room, whereas, during the second part, up to five people entered progressively in the room.

In order to obtain the ground-truth data, two additional equipment were used: 1) a Time-Of-Flight (TOF) camera mounted on the same tripod together with the RSS at the height of 3.00 m above the floor, and 2) a sensorized t-shirt worn by each participant. The TOF camera, SwissRanger SR4000 [38], was used to accurately capture information about person's position and movements inside the room, and to automatically annotate starting and ending time of each simulated action, i.e., change of body posture, as well as the occupancy level of the room (i.e., people counting). The SR4000 is a state-of-the-art TOF-based depth camera, having small dimensions

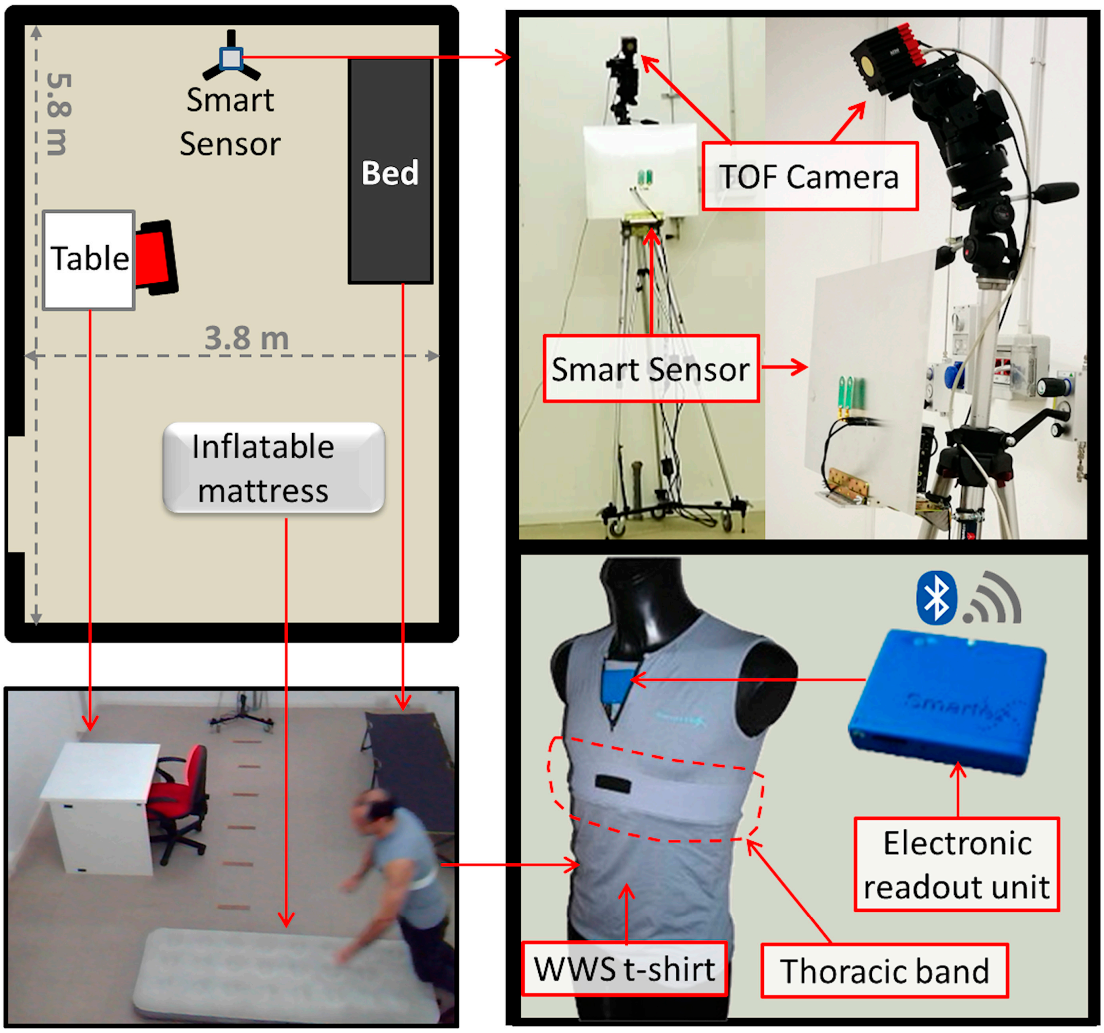

Figure 8. Experimental setup used for validating the RSS. A laboratory room (left-hand side) was equipped with movable furniture parts needed to simulate common ADLs and fall events. Ground-truth data were obtained by using a TOF camera and a WWS t-shirt (right-hand side).

Preprints (www.preprints.org) | NOT PEER-REVIEWED | Posted: 17 October 2017 doi:10.20944/preprints201710.0115.v1

Peer-reviewed version available at Biosensors 2017, 7, 55; doi:10.3390/bios7040055

(65×65×68 mm) and noiseless operation, able to provide QCIF (176×144 pixels) depth maps at high frame rate (up to 50 fps) within a wide Field-of-View (FoV) (69°×56°) and long distance range (up to 10 meters). Depth maps provided by the SR4000, after conversion into 3D point clouds, were used to automatically detect and count people present in the laboratory room, by using a high-performing approach which did not need to track one person at a time (i.e., tracking-free approach), but on the contrary it was able to detect and track all persons' location at the same time on the basis of an agglomerative clustering method [39]. Secondly, starting and ending times of each performed action were automatically identified by decomposing (classification task) the action into a sequence of hierarchical postures [40] (starting from four basic postures, namely, standing, bending, sitting, lying down) on the basis of high-discriminative features extracted from point clouds [41].

Regarding the ground-truth of cardiorespiratory data, during the data collection, each participant was wearing a WWS (Wearable Wellness System) t-shirt manufactured by Smartex [42], as shown in the bottom part of Figure 8, equipped with various sensors which provided precise measurements for HR and RR, thanks to the presence of a thoracic band including two textile ECG electrodes and one respiration sensor. In addition, the WWS t-shirt is equipped with a tri-axial accelerometer which provided information about body's movements useful to supplement that obtained using the SR4000 TOF camera. The HR and RR data measured by the SSS, during the experiments, were validated by comparing them with those measured by the WWS t-shirt. Such comparison was drawn in terms of accuracy measure, defined as the complementary of the mean relative error (MRE) given by $\mathrm{MRE} = \frac{1}{N}\sum_{n=1}^{N}\frac{|M_n^{SSS}-M_n^{WWS}|}{M_n^{WWS}}$, where M_n^{SSS} and M_n^{WWS} were the n-th measurements of M, which might be either HR or RR, provided by the SSS and WWS, respectively.

Regarding the micro-motion signature, the RSS was validated against a typical assisted living application, i.e., fall detection. At this purpose, the micro-motion signatures captured during the experiments were analysed using two main approaches [43]: supervised and unsupervised. The supervised one is the traditional approach for fall detection, in which a classifier is trained with both positive (i.e., simulated falls) and negative (i.e., ADLs) events. Since it is not realistic to assume that the classifier could be trained with falls simulated by end-users, normally the classifier is trained and tested with falls simulated by people having very different physical characteristics. In this study, the classifier was trained with falls simulated by individuals belonging to the young group, and tested with falls simulated by the older group. The unsupervised approach aims to overcome the lack of (real) fall data in training process, by considering falls as anomalous events. In such a way, the system can be trained to recognise "normal" events from sensor data captured during the end-user's ADLs, whereas falls are detected as anomalies, i.e., events diverging from the observed "normal" behaviour. In this case, during validation, the same participant can be involved in both training (simulating ADLs) and testing phases (simulating ADLs and falls). In this study, for both supervised and unsupervised approaches, a one-class Support Vector Machine (OCSVM) classifier [44] with Radial Basis Function (RBF) kernel was used and trained either with simulated falls or ADLs, respectively.

The fall detection performance was evaluated in terms of true positive rate (TPR) (or sensitivity) and true negative rate (TNR) (or specificity) measures [8], which definitions are based on the counting of true positives (TP), true negatives (TN), false positives (FP) and false negatives (FN), as follows: $\mathrm{TPR} = \frac{TP}{TP+FN}$, $\mathrm{TNR} = \frac{TN}{TN+FP}$. Furthermore, the ROC analysis was performed to determine the best performance at the varying of all the relevant parameters, such as those related with micro-Doppler spectrogram and OCSVM classifier.

3. Results and discussion

In general, the quality of both cardiac and respiratory signals detected by the RSS resulted quite good in comparison with the corresponding ground-truth signals, as illustrated in Figure 9 and Figure 10 respectively. However, the cardiac detection was more sensitive to movements than the

Preprints (www.preprints.org) | NOT PEER-REVIEWED | Posted: 17 October 2017 doi:10.20944/preprints201710.0115.v1

Peer-reviewed version available at Biosensors 2017, 7, 55; doi:10.3390/bios7040055

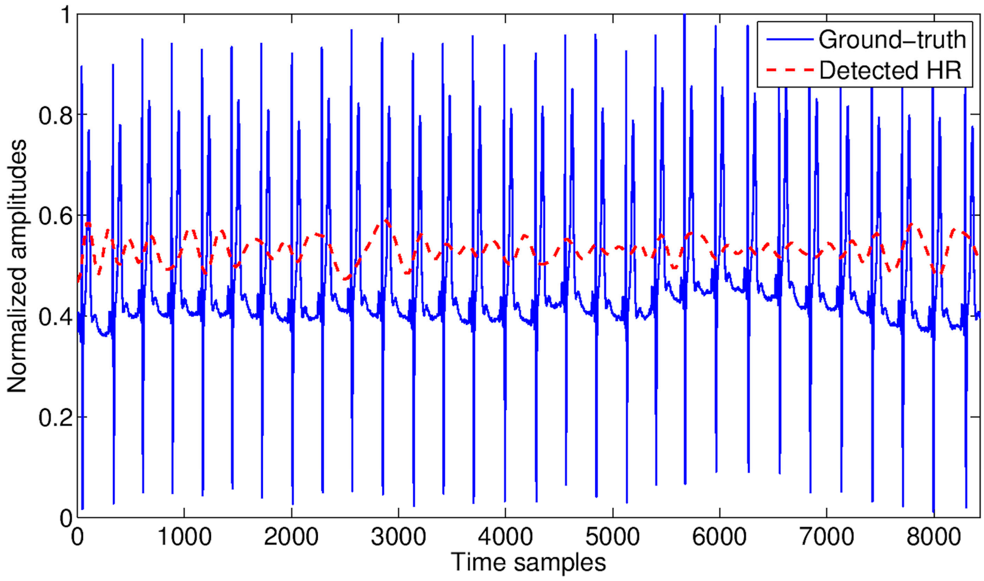

Figure 9. HR measured by the WWS (blue solid line) and by the RSS (red dashed line) via EMD at the distance person-sensor of 2 m. The peaks appearing in the ground-truth signal correspond to the 'R' waves.

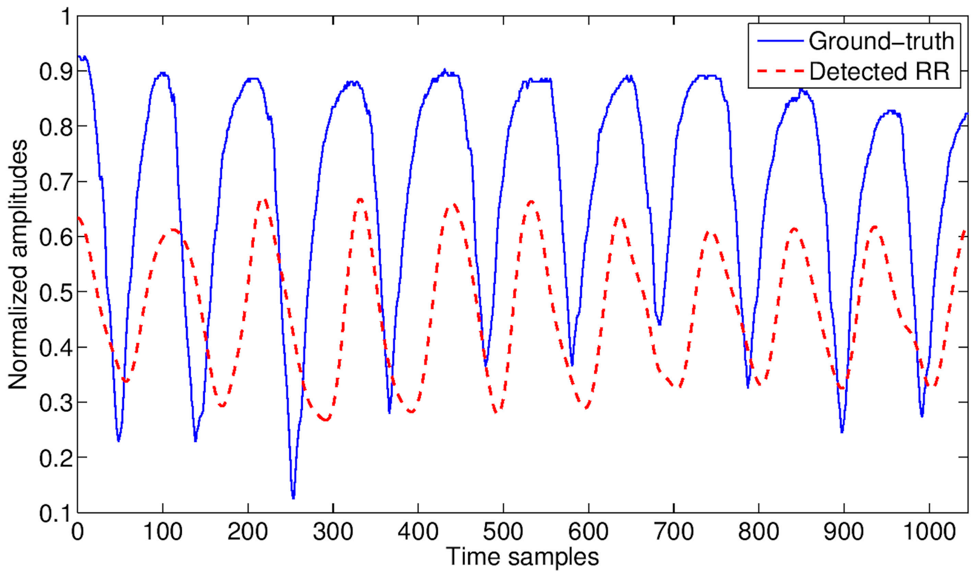

Figure 10. RR measured with WWS (blue solid line) and by the RSS (dashed line) via EMD at the distance person-sensor of 2 m.

respiratory one (especially to chest movements), resulting detectable only up to 3 m from the RSS. Beyond this limit, the EMD-based signal extraction strategy was not able to restore the SNR loss at the necessary level to separate the cardiac signal from the much stronger respiratory one. On the other hand, the respiratory signal resulted detectable with good accuracy up to 5 m from the sensor.

As mentioned above, the accuracy of the RSS to detect vital signs was evaluated in correspondence to some ADLs involving the three basic postures standing, sitting and lying down. In particular, the ADLs participants performed whilst in standing posture were cooking, preparing meals, and washing dishes, referred simply as "cooking" for short. The ADLs related to the sitting posture were eating at the kitchen table (referred simply as "eating"), and sitting on the couch

Peer-reviewed version available at *Biosensors* **2017**, *7*, 55; doi:10.3390/bios7040055

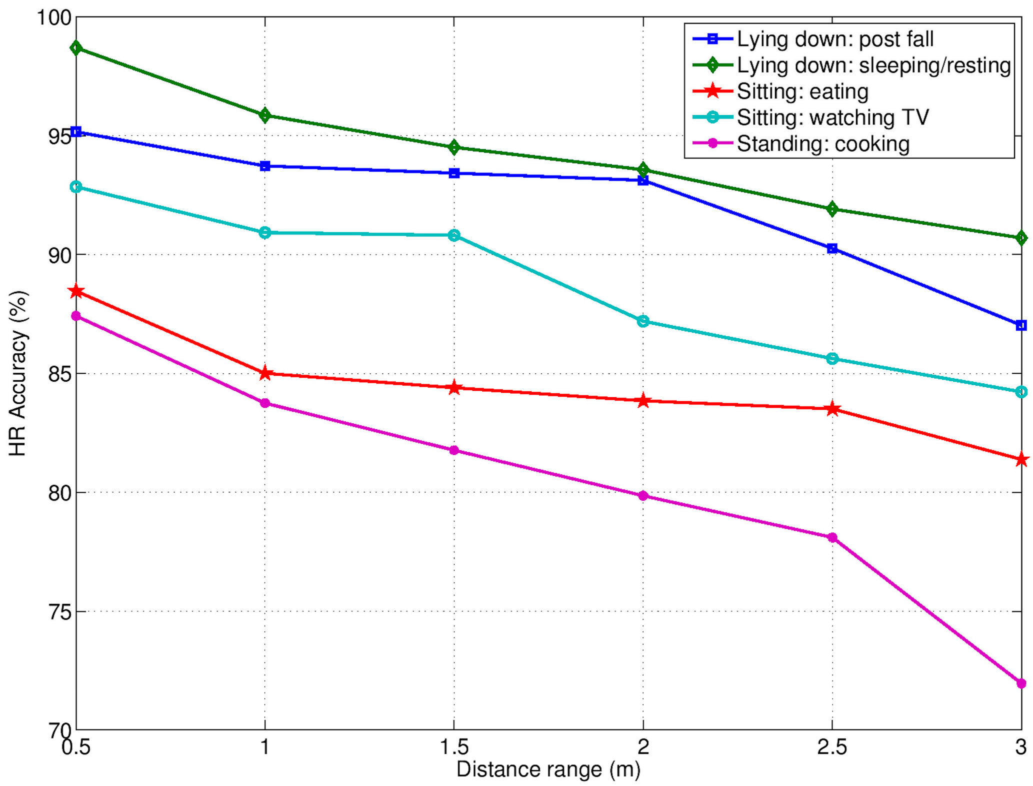

408 **Figure 11.** Accuracy of HR detection at varying of distances and ADLs. The only monitored subject
409 was present in the scene.

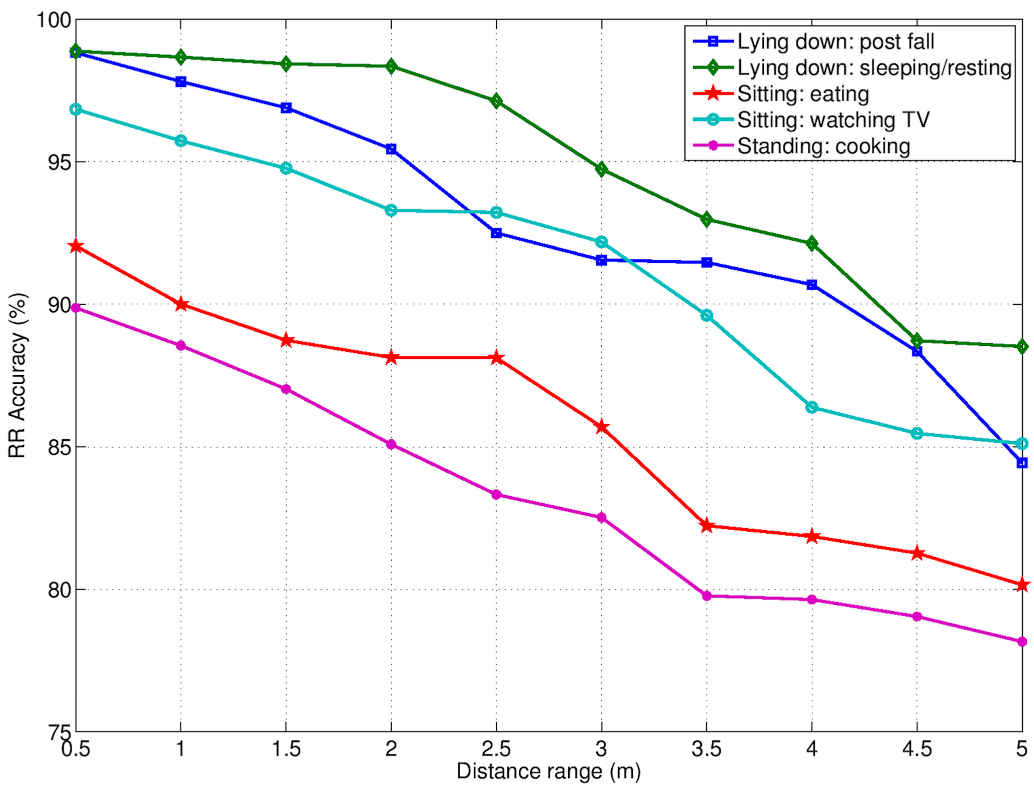

410 **Figure 12.** Accuracy of RR detection at varying of distances and ADLs. The only monitored subject
411 was present in the scene.

412 **Table 2.** HR and RR average accuracy achieved during ADLs and post-fall phase.

Activity	HR Accuracy (%)	RR Accuracy (%)
Lying down: post fall	89	93
Lying down: sleeping/resting	91	95
Sitting: eating	80	86
Sitting: watching TV	84	91
Standing: cooking	74	83
Average value	84	90

413 watching TV (referred simply as "watching TV"). Regarding the lying-down posture, it was taken
414 either during sleeping/resting or during the post-fall phase. In Figure 11 and Figure 12, the detection
415 accuracies for HR and RR, obtained in presence of the only monitored subject (i.e., only one person
416 in the room), are reported respectively. In both RR and HR cases, the best accuracy was achieved in
417 correspondence of ADLs/postures without too much movements, such as, sleeping/resting, post fall,
418 and watching TV. This explains the poor performance observed during the cooking (standing
419 posture) activity in comparison to the other ADLs. The same applied, although at a lesser extent, in
420 the case of the eating activity, due to some occurrence of chest oscillations. The average HR and RR
421 accuracies for each ADLs are summarized in Table 2. Some differences were found also in
422 dependence of the monitored subject's orientation. Especially in the case of HR, the most favourable
423 orientation was toward the sensor. The subject's position with respect to the radar antenna FoV (of
424 about 100°) was also relevant, since the detection accuracy decreased as the subject moved away
425 from the radial direction.
426 When more people were present in the RSS FoV (in addition to the monitored subject), the
427 movement compensation strategy was robust enough as long as the distance between the monitored
428 subject (i.e., the person closer to the RSS) and the other people was greater than 0.5 m. In such
429 conditions, the average losses in accuracy of about 2.61% and 4.88% were observed for HR and RR,
430 respectively, within the same distance ranges as before. The same data collection was used to
431 evaluate the RSS performance in detecting body's movements. To this end, micro-motion signatures
432 and distances detected by the RSS during each validation sequence were compared with
433 ground-truth data provided by the TOF camera. The micro-motion signatures were able to
434 characterize well body's movements in relation with performed actions, as shown in Figure 13
435 where a portion of sequence including a fall event is reported. As one can notice, the fall event

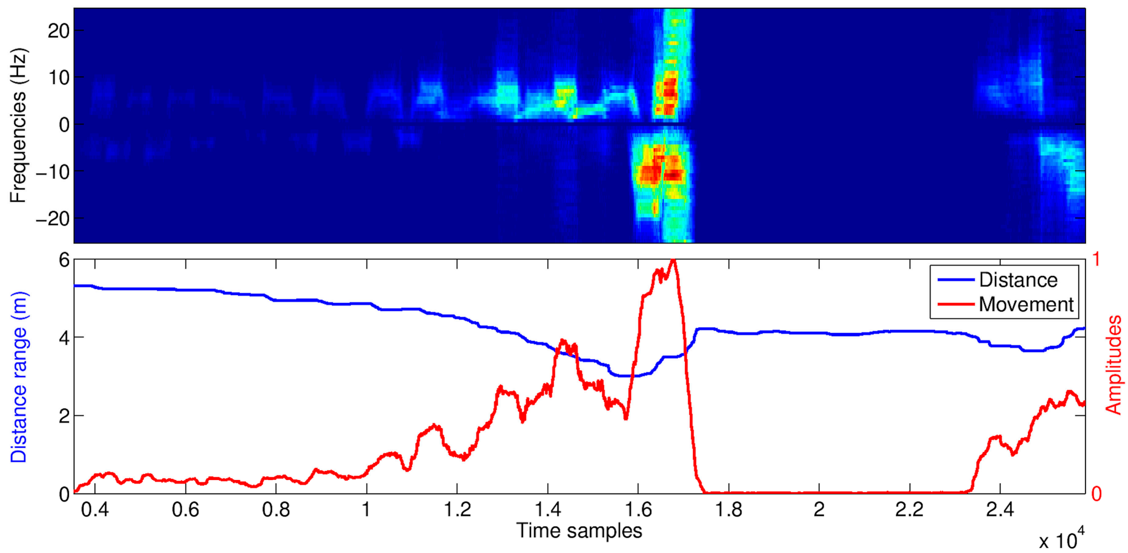

436 **Figure 13.** Micro-motion signatures (top side), distances and movement amplitudes (bottom side)
437 detected by the RSS during a validation sequence including a fall event (starting at the time sample
438 T=16000).

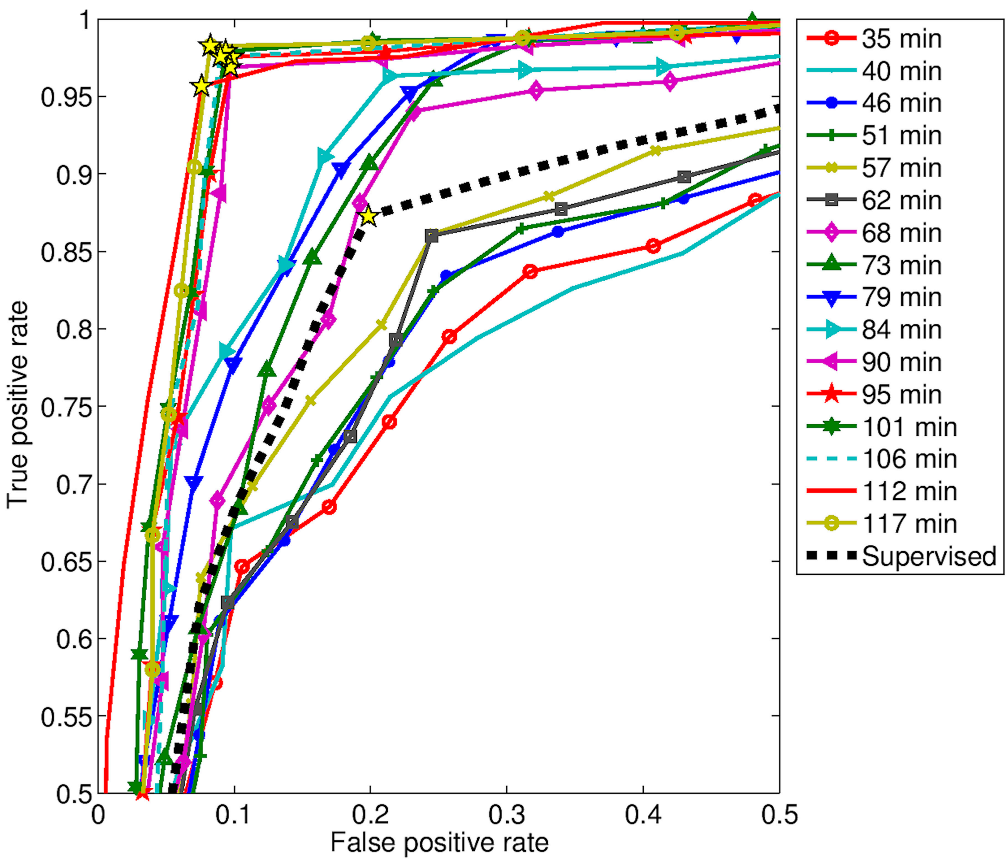

Figure 14. ROC analysis of the two detection approaches, unsupervised (for different training durations) and supervises.

occurred around the time sample T=16000 can be clearly distinguished from the previous walking actions. After the fall event, there was a time period during which the subject remained unmoving until the time sample T=24000 when the subject recovered from the fall. Further evidence about the effectiveness of micro-motion signatures in describing body's movements was obtained from the evaluation of the fall detection performance.

The achieved performance was quite different for the two approaches, supervised and unsupervised. More specifically, the unsupervised performance was dependent on the duration of the training phase based on "usual" ADLs. Roughly speaking, the longer lasted the unsupervised training, the higher was the detection performance.

In particular, the performance of the unsupervised approach overcame that of the supervised one, when the duration of the unsupervised training was greater than 68 min. The detection performance achieved with both approaches are summarized in Table 3, considering different training duration in the unsupervised case. The experimental data were evaluated using ROC analysis in order to accommodate various computational parameters. In the unsupervised case, a ROC curve was produced at each training duration, as displayed in Figure 14 starting from a duration of 35 min.

As one can notice, the unsupervised ROC curves are grouped into three groups. The first group includes the curves from 35 min. to 57 min., the second one from 68 min. to 84 min., and the third one from 90 min. to 117 min. The curve related to the supervised approach is placed in between the first and the second groups. From these results, hence, the following considerations can be drawn. The micro-motion signatures provided by the RSS are enough discriminative features suitable for event detection. However, their discriminative power can be improved at the cost of a greater inter-subject variability, as was done for example with the unsupervised learning approach.

4. Conclusions

The aim of this study was to develop and validate a RSS based on UWB-IR sensing, suitable for AAL applications. At this purpose, a comprehensive algorithmic framework for detection of both cardiorespiratory and body movements was presented and the related experimental results reported. The presented RSS was realistically evaluated by considering the detection of vital signs during the execution of various ADLs and also in presence of more than one moving subjects. Moreover, such detection capabilities were also evaluated for detecting falls and the fallen subject's vital signs during the post-fall phase. To this end, 30 healthy volunteers divided into two aged groups were involved by simulating both ADLs and falls events, at different distances, orientations and positions with respect the RSS. The achieved results show that vital signs can be reliable detected during some ADLs and during the post-fall phase, although with accuracy varying greatly depending on the level of movements and involved body's parts. The radar returns caused by movements of other people nearby were effectively compensated without significant loss of accuracy.

Furthermore, the experimental results also show the suitability of the RSS micro-movement signatures for fall detection, showing in particular the inter-subject variability which leaves room to user-customization approaches based on unsupervised learning. In conclusion, the original contribution of this work is twofold. Firstly, the promising UWB technology has been exploited for both fall detection and in-home unobtrusive vital signs monitoring. To the best of the authors' knowledge, this is the first study that demonstrated the feasibility of detecting falls and vital signs together, using micro-Doppler spectrograms through UWB radar sensing. Secondly, the ability of the suggested micro-motion signature to effectively discriminate between ADLs and falls has been demonstrated by means of an unsupervised detection, additionally allowing to deal with the problem of the lack of fall data for training. To the best of the authors' knowledge, in the literature few studies attempted to do so, but using wearable or acoustic sensors. The ongoing work is focused on further investigating the presented RSS in multi-sensor and multi-target real-life scenarios (e.g., community dwelling of older people) for simultaneous detection of vital signs and critical events.

Acknowledgments: This work was carried out within the project "ACTIVE AGEING AT HOME" funded by the Italian Ministry of Education, Universities and Research, within the National Operational Programme for "Research and Competitiveness" 2007-2013.

Table 3. This is a table. Tables should be placed in the main text near to the first time they are cited.

Approach	Training (min.)	Sensitivity (%)	Specificity (%)
Unsupervised	35	79.49	74.23
	40	75.61	78.56
	46	83.42	74.44
	51	82.41	75.39
	57	86.14	75.41
	62	86.01	75.53
	68	88.10	80.79
	73	90.63	80.1
	79	90.34	82.16
	84	91.10	83.44
	90	96.89	90.28
	95	97.56	90.16
	101	97.91	90.63
	106	97.57	91.02
	112	95.66	92.39
	117	98.26	91.75
Supervised	N.A.	87.27	80.15

Peer-reviewed version available at *Biosensors* **2017**, *7*, 55; doi:10.3390/bios7040055

Conflicts of Interest: The authors declare no conflict of interest. The founding sponsors had no role in the design of the study; in the collection, analyses, or interpretation of data; in the writing of the manuscript, and in the decision to publish the results.

References

1. United Nations, Department of Economic and Social Affairs, Population Division. World Population Prospects: The 2015 Revision, Volume II: Demographic Profiles. ST/ESA/SER.A/380. [Online]. Available: https://esa.un.org/unpd/wpp/Publications/Files/WPP2015_Volume-II-Demographic-Profiles.pdf
2. World Health Organization, Media centre. Falls - Fact sheet. Reviewed September 2016. [Online]. Available: http://www.who.int/mediacentre/factsheets/fs344/en/
3. Centers for Disease Control and Prevention, Injury Prevention & Control: Data & Statistics 2014. [Online]. Available: http://www.cdc.gov/injury/wisqars/
4. Rantz, M.J.; Skubic, M.; Miller, S.J. Using sensor technology to augment traditional healthcare. Proceedings of the 31st Annual International Conference of the IEEE Engineering in Medicine and Biology Society: Engineering the Future of Biomedicine, EMBC 2009, pages 6159–6162, 2009.
5. Lord, S.; Sherrington, C.; Menz, H.; Close, J. Falls in older people: risk factors and strategies for prevention (2nd ed.) Cambridge University Press, Cambridge, **2007**
6. Bergland, A.; Laake, K. Concurrent and predictive validity of “getting up from lying on the floor.” Aging Clin Exp Res **2013**; 17:181–185
7. Bloch, F. Critical falls: why remaining on the ground after a fall can be dangerous, whatever the fall. J Am Geriatr Soc **2012**; 60:1375–1376
8. Noury, N.; Rumeau, P.; Bourke, A.; OLaighin, G.; Lundy, J. A proposal for the classification and evaluation of fall detectors. Irbm **2008**; 29(6):340-349
9. Janssens, J.P.; Pautex, S.; Hilleret, H.; Michel, J.P.. Sleep disordered breathing in the elderly. Aging Clinical and Experimental Research, 12(6):417–429, 2000.
10. Casolo, G.; Balli, E.; Taddei, T.; Amuhasi, J.; Gori, C. Decreased spontaneous heart rate variability in congestive heart failure. The American Journal of Cardiology, 64(18):1162–1167, 1989.
11. Sajadieh, A.; Nielsen, O.W.; Rasmussen, V.; Hein, H.O.; Abedini, S.; Hansen, J.F. Increased heart rate and reduced heart-rate variability are associated with subclinical inflammation in middle-aged and elderly subjects with no apparent heart disease. European Heart Journal, 25(5):363–370, 2004.
12. Kooy, K.G.; Hout, H.P.J.; Marwijk, H.W.J.; Haan, M., C.D.A. Stehouwer, and A.T.F. Beekman. Differences in heart rate variability between depressed and non-depressed elderly. International Journal of Geriatric Psychiatry, 21(2):147–150, 2006.
13. Alonso, A.; Huang, X.; Mosley, T.H.; Heiss, G.; Chen, H. Heart rate variability and the risk of parkinson disease: The atherosclerosis risk in communities study. Annals of Neurology, 77(5):877–883, 2015.
14. Greneker, E.F. III. Radar sensing of heartbeat and respiration at a distance with security applica-tions. Proceedings of SPIE - The International Society for Optical Engineering, 3066:22–27, 1997.
15. Wild, K.; Boise, L.; Lundell, J.; Foucek, A.. Unobtrusive in-home monitoring of cognitive and physical health: Reactions and perceptions of older adults. Journal of Applied Gerontology, 27(2):181–200, 2008.
16. Malik, M.. Heart rate variability: Standards of measurement, physiological interpretation, and clinical use. Circulation, 93(5):1043–1065, 1996.
17. Hafner, N.; Lubecke, V. Performance assessment techniques for Doppler radar physiological sensors. Proceedings of the 31st Annual International Conference of the IEEE Engineering in Medicine and Biology Society: Engineering the Future of Biomedicine, EMBC 2009, pages 4848–4851, 2009.
18. Kumar M., Veeraraghavan A., and Sabharwal A.. Distanceppg: Robust noncontact vital signs monitoring using a camera. Biomedical Optics Express, 6(5):1565–1588, 2015.
19. Lubecke O.B., Ong P.-W., and Lubecke V.M.. 10 ghz doppler radar sensing of respiration and heart movement. Proceedings of the IEEE Annual Northeast Bioengineering Conference, NEBEC, 2002-January:55–56, 2002.
20. Immoreev I. and Tao T.-H.. Uwb radar for patient monitoring. IEEE Aerospace and Electronic Systems Magazine, 23(11):11–18, 2008.
21. Nguyen C, Han J. Time-Domain Ultra-Wideband Radar, Sensor and Components: Theory, Analysis and Design. Springer Science & Business Media, **2014**

22. Chen V.C., Li F., Ho S. S., Wechsler H. Micro-Doppler effect in radar: phenomenon, model, and simulation study. IEEE Transactions on Aerospace and electronic systems, 42(1), 2-21, 2006.
23. Amin MG, Zhang YD, Ahmad F, Ho KD. Radar signal processing for elderly fall detection: the future for in-home monitoring. IEEE Sig. Proc. Magazine 2016; 33(2):71-80.
24. Medrano C, Igual R, Plaza I, Castro M. Detecting falls as novelties in acceleration patterns acquired with smartphones. PloS one **2014**; 9(4):e94811.
25. Micucci D, Mobilio M, Napoletano P, Tisato F. Falls as anomalies? An experimental evaluation using smartphone accelerometer data. J Ambient Intell Humaniz Comput **2015**; 1-13
26. Lisowska A, Wheeler G, Inza V, Poole I. An Evaluation of Supervised, Novelty-Based and Hybrid Approaches to Fall Detection Using Silmee Accelerometer Data. In Proc. of IEEE CCVW **2015**; 10-16
27. Yuwono M, Moulton BD, Su SW, Celler BG, Nguyen HT. Unsupervised machine-learning method for improving the performance of ambulatory fall-detection systems. BioMedical Engineering Online **2012**; 11, 9.
28. Khana MS, Yua M, Fenga P, Wangb L, Chambersa J. An unsupervised acoustic fall detection system using source separation for sound interference suppression. Signal Processing **2015**; 110(May 2015):199–210
29. TIME DOMAIN. Pulson®p410 radar kit (2015, may 27). [Online] Available: http://www.timedomain.com/.
30. Abujarad F., Nadim G., and Omar A.. Clutter reduction and detection of landmine objects in ground penetrating radar data using singular value decomposition (SVD). Proceedings of the 3rd International Workshop on Advanced Ground Penetrating Radar, IWAGPR 2005, pp. 37–41, 2005.
31. Marple S. L.. Computing the discrete-time analytic signal via FFT. IEEE Trans. Signal Process., vol. 47, pp. 2600–2603, 1999.
32. Huang N.E., Shen Z., Long S.R., Wu M.L., Shih H.H., Zheng Q., Yen N.C., Tung C.C. and Liu H.H. The empirical mode decomposition and Hilbert spectrum for nonlinear and nonstationary time series analysis. Proc. Roy. Soc. London A, vol. 454, pp. 903–995, 1998.
33. Komaty A., Boudraa A. O., Augier B., Dare-Emzivat D.. EMD-based filtering using similarity measure between probability density functions of IMFs. In IEEE Trans. Instrum. Meas., vol. 63, no. 1, pp. 27-34, Jan. 2014.
34. Axiomtek. eBOX530-820-FL Fanless Embedded System Datasheet. [Online] Available http://www.axiomtek.it
35. Noury N, Rumeau P, Bourke A, OLaighin G, Lundy J. A proposal for the classification and evaluation of fall detectors. Irbm **2008**; 29(6):340-349.
36. Vlaeyen E, Deschodt M, Debard G, Dejaeger E, Boonen S, Goedemé T, Vanrumste B, Milisen K. Fall incidents unraveled: a series of 26 video-based real-life fall events in three frail older persons. BMC Geriatrics **2013**; 13:103.
37. Robinovitch SN, Feldman F, Yang Y, Schonnop R, Leung PM, Sarraf T, Sims-Gould J, Loughin M. Video capture of the circumstances of falls in elderly people residing in long-term care: an observational study. The Lancet **2013**; 381(9860):47-54.
38. HEPTAGON. [Online] Available: http://hptg.com/industrial
39. Diraco G.; Leone A.; Siciliano, P. People occupancy detection and profiling with 3D depth sen-sors for building energy management. In Energy and Buildings, 2015, 92: 246-266.
40. Diraco G.; Leone A.; Siciliano, P. In-home hierarchical posture classification with a time-of-flight 3D sensor. In Gait Posture, 2014, 39/1: 182-187.
41. Diraco G.; Leone A.; Siciliano, P. Geodesic-based human posture analysis by using a single 3D TOF camera. Industrial Electronics (ISIE), IEEE International Symposium on, 27-30 June, 2011.
42. SMARTEX. Wearable wellness system. [Online] Available: http://www.smartex.it/en/our-products/232-wearable-wellness-systemwws/
43. Khan, S.S.; Hoey, J. Review of fall detection techniques: A data availability perspective. In: Medical engineering & physics, vol. 39, pp. 12-22, 2017.
44. Yu, M.; Yu, Y.; Rhuma, A.; Naqvi, S. M. R.; Wang, L.; Chambers, J. A. An online one class support vector machine-based person-specific fall detection system for monitoring an elderly individual in a room environment. IEEE journal of biomedical and health informatics, vol. 17(6), pp. 1002-1014, 2013.